Deposition and properties of Fe(Se,Te) thin films on vicinal CaF_2 substrates

Deposition and properties of Fe(Se,Te) thin films on vicinal CaF_2 substrates

Hagen Bryja[1,2], Ruben Hühne[1], Kazumasa Iida[3], Sebastian Molatta[4], Alberto Sala[5], Marina Putti[5], Ludwig Schultz[1,2], Kornelius Nielsch[1,2] and Jens Hänisch[6]

[1] Institute for Metallic Materials, IFW Dresden, Dresden, Germany
[2] Institute of Materials Science, TU Dresden, Dresden, Germany
[3] Department of Materials Physics, Nagoya University, Nagoya, Japan
[4] Dresden High Magnetic Field Laboratory, Helmholtz Zentrum Dresden Rossendorf, Dresden, Germany
[5] Dipartimento di Fisica, Università di Genova and CNR SPIN, Genova, Italy
[6] Karlsruhe Institute of Technology, Institute of Technical Physics, Karlsruhe, Germany

E mail: h.bryja@ifw dresden.de

Abstract

We report on the growth of epitaxial $Fe_{1+\delta}Se_{0.5}Te_{0.5}$ thin films on 0°, 5°, 10°, 15° and 20° vicinal cut CaF_2 single crystals by pulsed laser deposition. *In situ* electron and *ex situ* x-ray diffraction studies reveal a tilted growth of the $Fe_{1+\delta}Se_{0.5}Te_{0.5}$ films, whereby under optimized deposition conditions the *c*-axis alignment coincides with the substrate [001] tilted axis up to a vicinal angle of 10°. Atomic force microscopy shows a flat island growth for all films. From resistivity measurements in longitudinal and transversal directions, the *ab*- and *c*-axis components of resistivity are derived and the mass anisotropy parameter is determined. Analysis of the critical current density indicates that no effective *c*-axis correlated defects are generated by vicinal growth, and pinning by normal point core defects dominates. However, for $H||ab$ the effective pinning centers change from surface defects to point core defects near the superconducting transition due to the vicinal cut. Furthermore, we show in angular-dependent critical current density data a shift of the *ab*-planes maxima position with the magnetic field strength.

Keywords: vicinal substrates, anisotropy, critical current density, $Fe_{1+\delta}Se_{0.5}Te_{0.5}$ thin films

Introduction

The discovery of superconductivity in the iron-based compound $LaFeAsO_{1-x}F_x$ (1111-system) with a critical temperature (T_c) of 26 K in the year 2008 [1] gained much interest in the scientific community, and many other iron-based superconductors such as doped $BaFe_2As_2$ (122-system) [2], FeSe (11-system) [3] and LiFeAs (111-system) [4] were found. In order to study this new class of superconductors, thin films are suitable for investigating the fundamental properties and potential applications due to their geometry. Furthermore, biaxial strain caused by lattice or thermal mismatched substrates can have a crucial impact on T_c in iron-based superconductors [5 9]. Nonetheless, previously published works on iron-based superconducting thin films only deal with films on plane-cut (001)-oriented substrates; the growth on vicinal cut substrates has to the best of our knowledge not been studied. For the cuprate-based superconductors $YBa_2Cu_3O_7$ (YBCO) [10], $Bi_2Sr_2CaCu_2O_8$ [11], $Bi_2Sr_2Ca_2Cu_3O_{10}$ [12], and $HgBa_2CaCu_2O_6$ [13] as well as MgB_2 [14], it has already been shown that vicinal cut substrates open access to many new experimental opportunities. By breaking the symmetry between substrate normal and crystallographic *c*-axis, it is possible to analyze the transport properties at a specific angle to the crystal lattice rather than just parallel to one of the crystallographic main axes, and therefore a new way to investigate electrical anisotropies is enabled. Vicinal cut substrates also offer a powerful tool to separate the influence

Table 1. Deposition temperatures and structural data for the films.

Series	T_{dep} (°C)	Vicinal angle β (°)	Growth angle β' (°)	c axis (Å)	Longitudinal $\Delta\omega_{003}$ (°)	Transversal $\Delta\omega_{003}$ (°)
1	260	0	0	6.02	1.8	1.8
	260	5	5	5.90	1.3	1.5
	260	10	7.6	5.88	1.6	3.8
	260	15	12	5.89	1.4	5.9
	260	20	17.6	5.90	2.0	7.1
2	400	0	0	6.00	0.9	0.9
	400	5	5	5.99	0.9	0.9
	400	10	10	5.87	0.7	0.7

of different pinning centers (e.g. *ab*-planar defects and surfaces) or create new ones (antiphase boundaries) in a controlled manner [10, 15]. This allows the mimicking of the geometry of thin films on technical substrates, such as ion-beam assisted deposition (IBAD) or inclined substrate deposition templates [16]. Indeed, $FeSe_{0.5}Te_{0.5}$ [17], Co-doped $BaFe_2As_2$ [18], and $NdFeAsO_{1-x}F_x$ [19] have been deposited on such usually slightly vicinal IBAD templates. In addition, it has been observed that the growth mode of YBCO films can change from island-type to step-flow by using vicinal cut $SrTiO_3$ substrates, leading to a more uniform and smoother film surface [20]. A change in porosity in vicinal YBCO nanocomposite thin films has also been observed [21].

In order to gain a deeper insight into the effects of vicinal growth of Fe(Se,Te) thin films and into the critical current density (J_c) and resistivity anisotropy, we investigated the preparation as well as the structural, morphological and physical properties of epitaxial $Fe_{1+\delta}Se_{0.5}Te_{0.5}$ thin films on CaF_2 single crystals cut at angles between 0° and 20° with respect to [001]. The 11-system is of particular interest because of the simple structure, moderate T_c of 14 K [22], low electronic anisotropy and high upper critical fields (H_{c2}) in the range of 50–100 T [23], providing a good model system to study superconductivity in iron-based superconductors and also to explore possible technological applications.

Experimental methods

Epitaxial $Fe_{1+\delta}Se_{0.5}Te_{0.5}$ thin films were grown on CaF_2 single crystals cut at angles β between 0° and 20° with respect to [001] by pulsed laser deposition using a KrF excimer laser (wavelength: 248 nm). The target was synthesized by a two-step method as described in detail in [24]: high purity small-grained powders of Fe, Se and Te were mixed in the stoichiometric ratio of Fe:Se:Te = 2:1:1, sealed in an evacuated Pyrex tube and heated up to 500 °C. A pellet of the reacted powder was melted in a sealed quartz tube with argon atmosphere using a high frequency induction furnace. The films were prepared with a laser repetition rate of 7 Hz under ultra-high vacuum with a base pressure of 10^{-9} mbar. The film growth was monitored by reflection high-energy electron diffraction (RHEED) for exemplary films. The vicinal cut substrates were annealed for 1 h at 850 °C in order to achieve a more uniform surface structure. Two different substrate temperatures during deposition (T_{dep}), 260 °C (series 1) and 400 °C (series 2), were investigated. The deposition temperature of 260 °C was motivated by [25, 26] as well as our own experience. During the course of the experiments, a deposition temperature around 400 °C turned out to be more suitable for $Fe_{1+\delta}Se_{0.5}Te_{0.5}$ films with high T_c and J_c [27]. Although a stoichiometric target was used, all films reveal reproducible indications of iron excess (estimated to be around 10% by comparing with literature data) including nonmetallic behavior as well as lower T_c and J_c values [28–31]. Therefore, a composition of $Fe_{1+\delta}Se_{0.5}Te_{0.5}$ is stated for the investigated samples.

The structural properties of the films were measured by x-ray diffraction (XRD) via a texture goniometer *Phillips X'pert* with Cu-K_α radiation. The c-axis lattice parameters were calculated from θ-2θ scans using the Nelson Riley function [32]. The thicknesses of the films were determined from cross sections prepared by focused ion beam (*FEI Helios* 600*i*) and estimated to be around 85 nm. The surface morphology was studied by atomic force microscopy (AFM) with an *Asylum Research Cypher S*.

For the films of series 1, 1 mm wide bridges were fabricated by conventional photolithography and ion-beam etching. The used cross type geometry allows the measurement of two perpendicularly intersecting current tracks. In one track the current flows parallel to the *ab*-planes (longitudinal direction) and in the other track the current has a perpendicular component with respect to the *ab*-planes (transversal direction) of the film. For the films of series 2, only the tracks in the longitudinal direction were prepared by cutting 1 mm wide bridges with a diamante pin. Silver paint was employed for electrical contacts. The superconducting properties were measured in a four-probe configuration in magnetic fields up to 9 T with a physical property measurement system (PPMS Quantum Design). The critical temperature is defined from resistive transition in zero field at a criterion of 90% (0%) of the normal state resistance, noted here as $T_{c,90}$ ($T_{c,0}$). A voltage criterion of 1 μVcm^{-1} was employed for evaluating J_c. Angular-dependent J_c measurements were performed in maximum Lorentz force configuration in longitudinal direction, with θ as the angle between the magnetic field direction and the surface normal of the film. The samples investigated in this study and their structural properties are summarized in table 1.

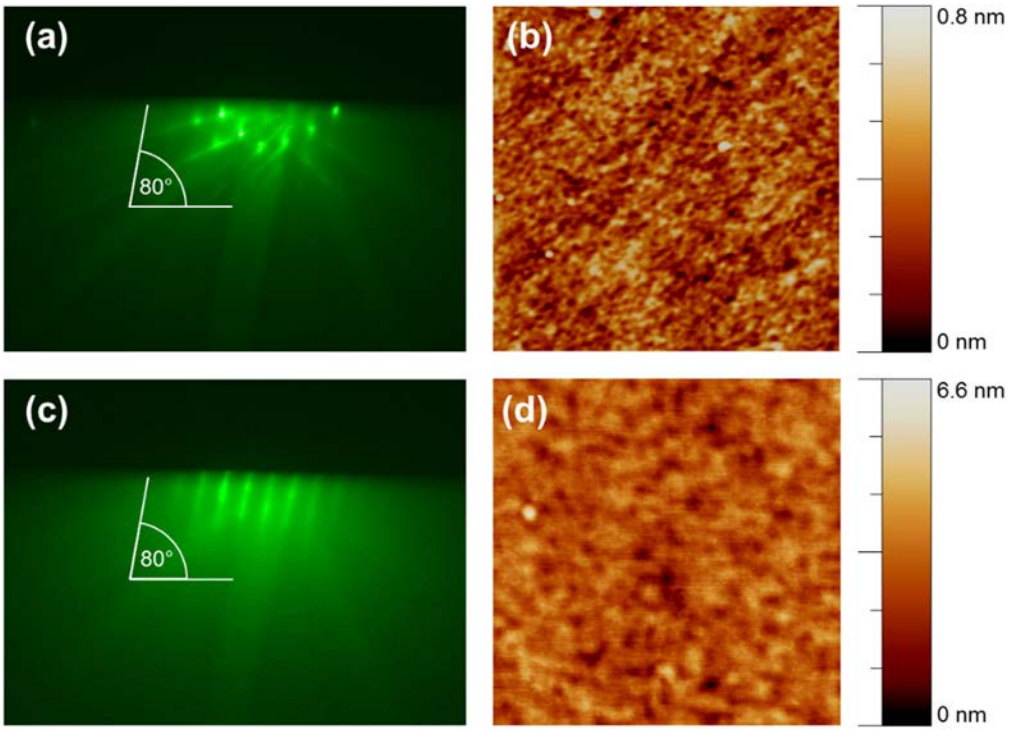

Figure 1. Surface orientation and surface morphology of a 10° vicinal cut CaF_2 substrate and $Fe_{1+\delta}Se_{0.5}Te_{0.5}$ thin film. (a) RHEED image of the substrate, (b) corresponding AFM image (5 μm × 5 μm). (c) RHEED image of the $Fe_{1+\delta}Se_{0.5}Te_{0.5}$ thin film deposited at 400 °C, (d) corresponding AFM image of the film surface (5 μm × 5 μm).

Results and discussion

Figure 1 compares surface crystal orientation by RHEED and surface morphology by AFM of a 10° vicinal cut substrate (a, b) with those of the grown film ($T_{dep} = 400$ °C, series 2) on that substrate (c, d). Both substrate and film show a tilt of 10° of the characteristic streaky RHEED patterns. The RHEED pattern of the film shows elongated spots along the *c*-direction, indicating a small but finite surface roughness. No terrace surface termination at the pristine (annealed) CaF_2 substrate surfaces was found. Consequently, the film surface also did not reveal a terrace structure. All films are very smooth with a slight increase in root mean square (rms) roughness for higher deposition temperature (series 2) and increasing vicinal angle. As an example, the rms roughness of the 10° vicinal film in series 2, shown in figure 1(d), is 0.64 nm. For all films, an island-type of growth instead of step-flow growth was found this is due to the absence of a clear terrace surface termination at the substrate surfaces.

Figure 2(a) shows the θ-2θ scan of the 10° vicinal film of series 2, measured with a ψ-offset of 10°. For all films only (00ℓ) reflections of the $Fe_{1+\delta}Se_{0.5}Te_{0.5}$ together with (00ℓ) reflections of the CaF_2 are observed, indicating *c*-axis oriented growth without signs of phase impurities. The lattice constants *c* of the thin films on 0° substrates (table 1) are smaller than those of $Fe_{1+\delta}Se_{0.5}Te_{0.5}$ single crystals ($a = 3.801$ Å, $c = 6.034$ Å) [22] (table 1), but in excellent agreement with the reported values for thin films of a Se:Te ratio of 1:1 on CaF_2 substrates [25, 27]. Since the *c*-axis parameters of the vicinal films are reproducibly and systematically further reduced, it seems the vicinal growth helps to sustain epitaxial strain in $Fe_{1+\delta}Se_{0.5}Te_{0.5}$ films, even in the absence of step-flow growth.

In order to check the tilted epitaxial growth, (202) pole figures of the CaF_2 substrates and (112) pole figures of the $Fe_{1+\delta}Se_{0.5}Te_{0.5}$ thin films were measured. Figure 2(b) shows the contour plots for the 10° vicinal substrate and film of series 2. All films reveal clear four-fold symmetry with a full 45° rotation with respect to the substrate. For the 5° vicinal film of series 1, the tilt angle of the film equals the vicinal angle of the substrate. However, for the film deposited on the 10° substrate the intensity maxima of the tilt angle (growth angle β') can be found at 7.6°, for the film on the 15° substrate at 12° and for the 20° substrate at 17.6°. In contrast, for the 10° film of series 2 the *c*-axis alignment coincides with the substrate [001] tilted axis. Too low a deposition temperature, therefore, leads to a systematic back-tilt towards the substrate normal, presumably due to surface energy minimization.

Rocking curves of the $Fe_{1+\delta}Se_{0.5}Te_{0.5}$ (003) peak were measured in longitudinal and transversal directions, as exemplarily shown for the 10° vicinal sample of series 2 in figures 2(c) and (d), respectively. The full width at half maximum (FWHM) values of these rocking curves for all thin films are summarized in table 1. They are not corrected for device broadening. For the films of series 1, the FWHM values in the longitudinal direction (longitudinal $\Delta\omega_{003}$) show no remarkable trend. In the transversal direction (transversal $\Delta\omega_{003}$), however, an increase with increasing vicinal angle is observed, indicating a larger spread of the *ab*-plane alignment. Films of series 2 show narrower rocking curves (see

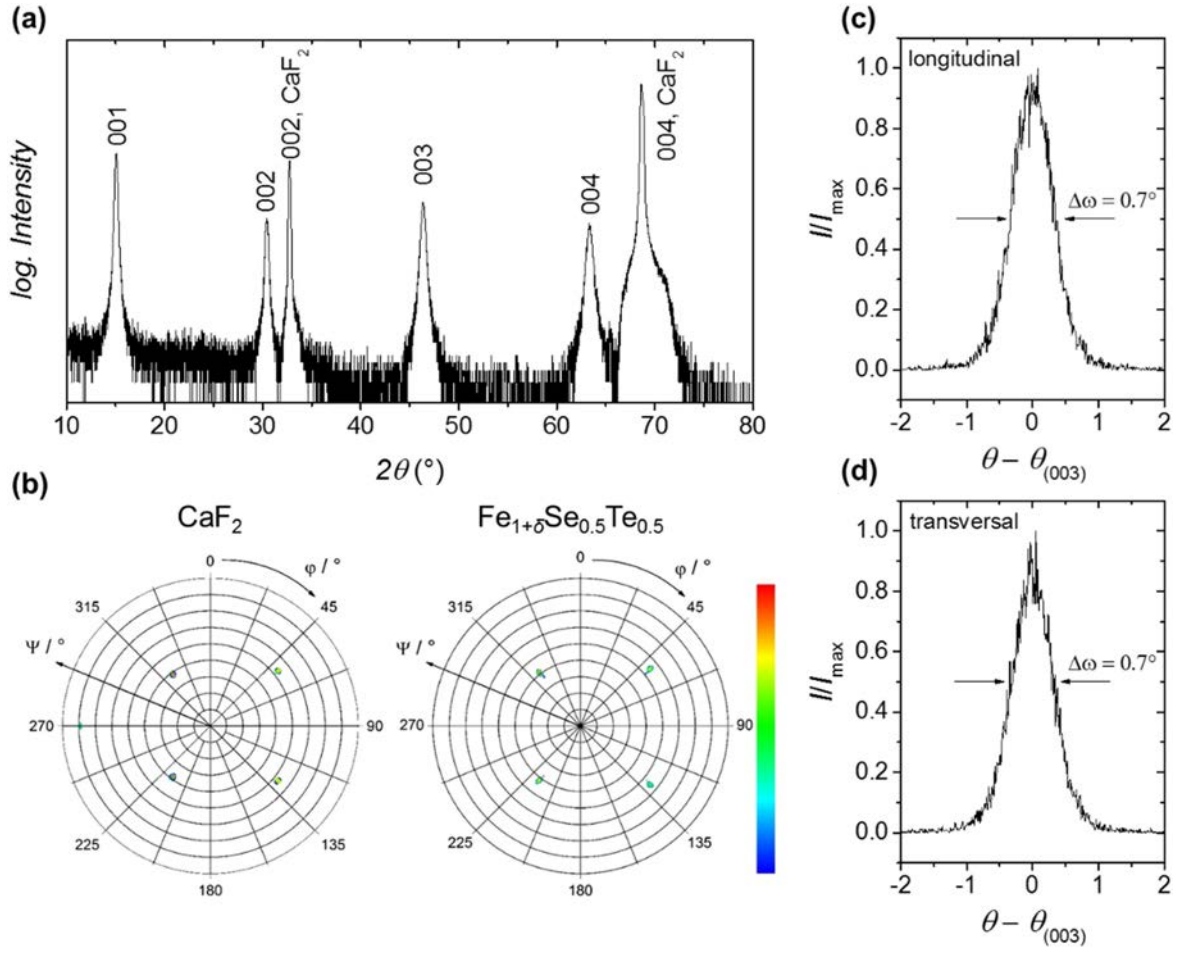

Figure 2. Phase purity and texture of the 10° vicinal $Fe_{1+\delta}Se_{0.5}Te_{0.5}$ thin film of series 2. (a) θ 2θ XRD scan. (b) Pole figures of the CaF_2 (202) and $Fe_{1+\delta}Se_{0.5}Te_{0.5}$ (112) reflection. Rocking curves of the $Fe_{1+\delta}Se_{0.5}Te_{0.5}$ (003) reflection in (c) longitudinal and (d) transversal direction.

also [27]) without a difference in the measured direction up to 10°, indicating a higher crystalline quality with better alignment due to the better phase formation at higher deposition temperatures. A similar effect has been reported by Huang *et al* for the in-plane texture on MgO substrates [25].

The temperature dependences of the resistivity (ρ) for the 5°, 15° and 20° vicinal $Fe_{1+\delta}Se_{0.5}Te_{0.5}$ films of series 1 are shown in figure 3(a). The resistivities in the longitudinal direction, ρ_L, of all vicinal films are similar in the entire temperature range (15 K 300 K) and show reproducibly nonmetallic behavior, i.e. increasing resistivity with decreasing temperature. The values and temperature dependences of ρ_L are similar to literature data on iron excess $Fe_{1+\delta}Se_{1-x}Te_x$ single crystals in the *ab*-direction [28]. In contrast, $FeSe_{1-x}Te_x$ without iron excess shows metallic behavior with lower resistivity values [28 31]. In the transversal direction, the current has to flow in a path along the tilted planes, containing an *ab*- and *c*-axis component. Consequently, due to the intrinsic anisotropy of $Fe_{1+\delta}Se_{0.5}Te_{0.5}$, the measured resistance in the transversal direction ρ_T is higher than in the corresponding longitudinal direction for every film. In the plot of normalized resistance over temperature (figure 3(b)), it is also obvious that ρ_T curves show a systematically increasing upturn with higher vicinal angle due to the increased *c*-axis component.

The inset of figure 3(b) shows the enlarged view of the normalized superconducting transitions. With increasing vicinal angle, T_c decreases, whereby the transversal directions show a lower $T_{c,0}$ than the respective longitudinal directions and hence a larger transition width. This is presumably due to a vicinal-angle-dependent inhomogeneous excess iron distribution in the films caused by low deposition temperature.

The *c*-axis resistivity ρ_c can be calculated using the rotation of the resistivity tensor by the vicinal growth angle β' (table 1) according to the expression: $\rho_c = (\rho_T - \rho_L \cos^2\beta')/(\sin^2\beta')$ [11]. The results are shown in figure 3(c). The calculated $\rho_c(T)$ data also indicate nonmetallic behavior. ρ_c of the film on 5° vicinal cut substrate is close to single crystal values of $FeSe_{0.4}Te_{0.6}$ [33], although the temperature dependence differs, which is explained by the iron excess [28]. The calculated ρ_c values of the films on 15° and 20° vicinal cut substrates are significantly lower, which should not be the case for optimally aligned and defect-free films. The reason is a decreased transverse resistivity due to the larger orientation spread in this direction for these films. Due to the much lower resistivity in

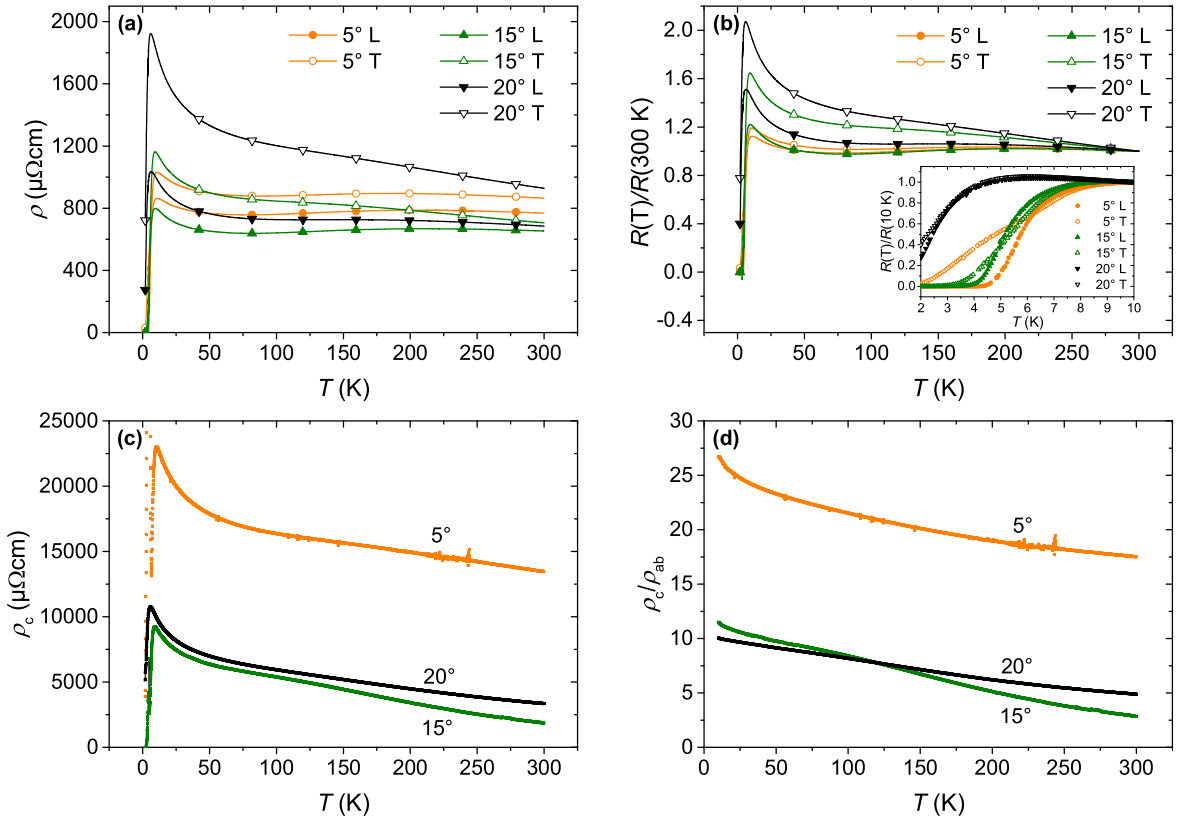

Figure 3. The temperature dependence of the resistivity of the 5°, 15° and 20° vicinal $Fe_{1+\delta}Se_{0.5}Te_{0.5}$ thin films of series 1. (a) Resistivity versus temperature in longitudinal and transversal directions. (b) Normalized resistivity versus temperature plots. The inset shows normalized resistivity traces. (c) Temperature dependence of ρ_c. (d) Temperature dependence of the resistivity anisotropy ρ_c/ρ_{ab}.

the *ab*-direction, small portions of misaligned grains already lead to a strong reduction of ρ_T.

From the resistance ratio ρ_c/ρ_{ab} (figure 3(d)), it is possible to obtain the mass anisotropy parameter γ near the superconducting transition, according to the equation: $\gamma = H_{c2}^{\parallel}/H_{c2}^{\perp} = \sqrt{m_c^*/m_{ab}^*} = \sqrt{\rho_c/\rho_{ab}}$, by assuming that $\rho_{ab} = m_{ab}^*/ne^2\tau$ and $\rho_c = m_c^*/ne^2\tau$ applies [33], where n is the carrier concentration, e is the electric charge, τ is the relaxation time of carriers, and m_{ab}^* and m_c^* are the effective masses in the *ab*-plane and along the *c*-axis, respectively. The value of γ thus obtained for the 5° vicinal film is 5.2 just above T_c, which is in good agreement with reported values estimated from the anisotropy of H_{c2} from $FeSe_{0.5}Te_{0.5}$ thin films and single crystals [27, 34, 35]. Due to the microstructure-induced reduction of ρ_T, the films grown at higher vicinal angles show apparent lower anisotropy parameters with $\gamma = 3.2$ and $\gamma = 3.4$ near T_c for the 15° and 20° vicinal film, respectively.

The films of series 2, deposited at 400 °C, were used to investigate the critical current density of vicinal $Fe_{1+\delta}Se_{0.5}Te_{0.5}$ thin films. The film deposited on the 0° substrate shows a $T_{c,90}$ ($T_{c,0}$) of 15.5 K (13.3 K) and the film on the 5° substrate a $T_{c,90}$ ($T_{c,0}$) of 17.0 K (15.2 K). The film on the 10° substrate has a reduced $T_{c,90}$ ($T_{c,0}$) of 10.3 K (5.7 K). No correlation between T_c and the *c*-axis constants of the films was found.

For the 0° and 5° vicinal thin films with high T_c, we measured J_c in a longitudinal direction at several temperatures for $H||c$ and $H||ab$, as shown in figure 4. The 0° film shows a self-field J_c of 42 kA cm ^{2} at 4.2 K, whereas the 5° vicinal film shows a slightly lower self-field J_c of 30 kA cm ^{2} despite the higher T_c. These values are approximately one order of magnitude lower compared to stoichiometric $FeSe_{0.5}Te_{0.5}$ films on CaF_2 [26, 36 38] due to iron excess and reduced T_c. Both films show a fast decrease in J_c for $H||c$ at temperatures above $T_c/2$. J_c for $H||ab$ shows a weaker dependence on the applied field. Obviously, the flux pinning for both films is anisotropic. At low temperatures, the 0° sample shows higher J_c values in the whole magnetic field range investigated. At high temperatures, however, the 5° sample shows higher J_c values for the same temperature. This is not an effect of vicinality but of the difference in T_c. At temperatures corresponding to nearly the same T/T_c value (i.e. the pairs 8 K/10 K and 10 K/12 K) magnitude and field dependence of J_c are very similar.

Figure 5 compares the corresponding normalized pinning force densities $f_p \sim h^p(1-h)^q$, $f_p = F_p/F_{p,max}$, where $F_{p,max}$ is the maximum pinning force density and $h = H/H_{irr}$ is the reduced magnetic field with respect to the irreversibility field H_{irr}. The $H||c$ data of the 0° film fall approximately on a single curve with $p = 1.02$ and $q = 2.04$ in a broad temperature range. These values are very close to the expected values $p = 1$ and $q = 2$ for normal core point pinning [39]

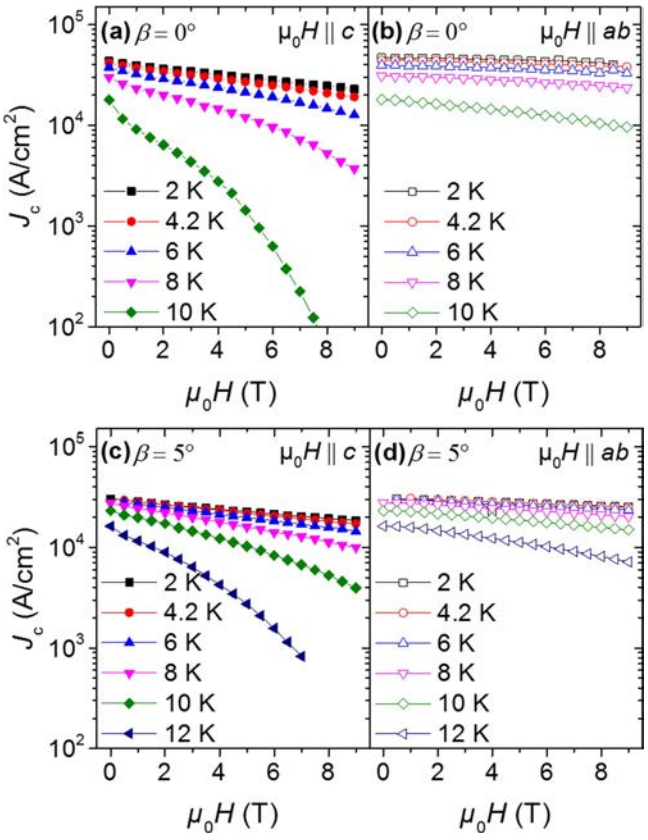

Figure 4. Magnetic field dependence of the critical current densities in longitudinal direction for $Fe_{1+\delta}Se_{0.5}Te_{0.5}$ thin films of series 2 with vicinal angle $\beta = 0°$ for (a) $H||c$ and (b) $H||ab$ and $\beta = 5°$ for (c) $H||c$ and (d) $H||ab$.

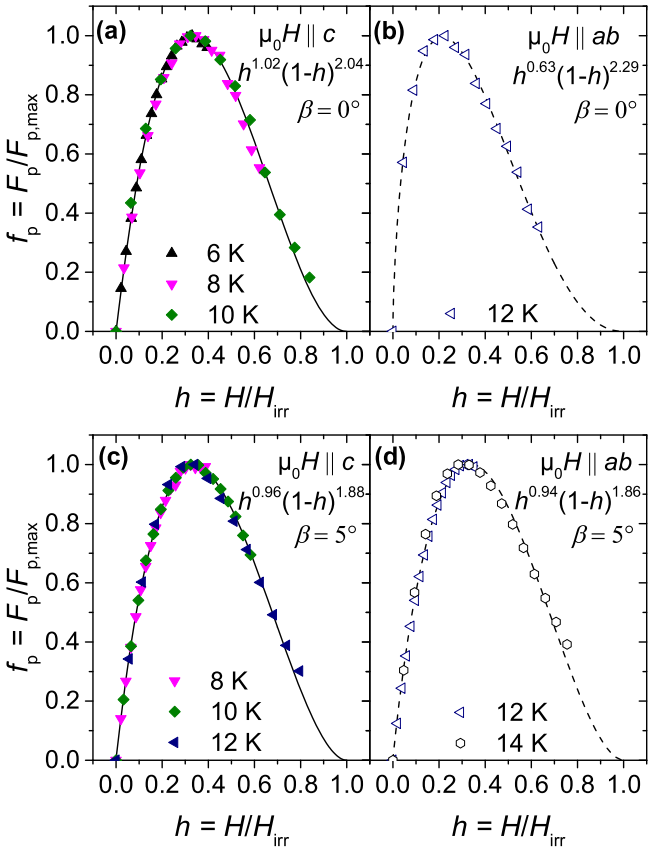

Figure 5. Normalized pinning force f_p as a function of the reduced magnetic field h in the longitudinal direction for $Fe_{1+\delta}Se_{0.5}Te_{0.5}$ films of series 2 with vicinal angle $\beta = 0°$ for (a) $H||c$ and (b) $H||ab$ and $\beta = 5°$ for (c) $H||c$ and (d) $H||ab$.

and in agreement with reports on stoichiometric Fe(Se,Te) thin films [40 42]. The $H||c$ data of the 5° vicinal film can be fitted with similar values $p = 0.95$ and $q = 1.85$. This indicates the same pinning mechanism dominates in both films, and no additional pinning by surface defects ($p = 0.5$ and $q = 2$) as expected for grain boundaries is induced in c-axis direction by the vicinal growth. The absence of flat terraces on the vicinal CaF_2 substrates (in contrast to vicinal $SrTiO_3$ substrates with single termination) seems to hinder the formation of antiphase boundaries and grain boundaries in the c-direction. This has to be confirmed by transmission electron microscopy investigations in the future.

Due to the limited available magnetic field, for $H||ab$ only J_c at temperatures near the superconducting transition was used for scaling. Nonetheless, for the 0° film the $f(h)$ dependence at 12 K with $p = 0.63$ and $q = 2.29$ points to a pinning rather dominated by surface defects, indicating an influence of extended ab-planar defects. In contrast, for the 5° vicinal film we found $p = 0.94$ and $q = 1.86$ for $H||ab$ and therefore pinning dominated by point defects.

The comparison of the $J_c(\theta)$ dependencies between the 0°, the 5° and the 10° film (figure 6) illustrates the effect of the vicinal growth on J_c. For all films, we found a maximum in J_c for $H||ab$, whereby the ab-planes of the films were determined from the position of the ab-peak at high magnetic fields (9 T). The 0° film displays a weak field dependence in this direction, in accordance with the enhanced pinning by extended ab-defects as determined by the F_p analysis for high temperatures. The vicinal films show a stronger field dependence for $H||ab$, although the curves also indicate that pinning by extended planar defects is present at lower temperatures. The slight asymmetry in the ab-peak is attributed to the broken symmetry, i.e. the angle between film surface and crystallographic ab-plane. This effect is further investigated on the 10° film below. With the exception of the 1 T $J_c(\theta)$ curve for the 5° film which shows a slightly maximum for $\theta \approx 180°$, no clear further peaks are visible for all films. In contrast, Maiorov *et al* observed for YBCO films on tilted IBAD-MgO-tapes a distinct J_c peak positioned close to the surface normal, which had its origin in edge dislocations between the grains growing perpendicular to the surface [43].

Figure 7(a) shows the enlarged view of the ab-peak of the 10° film from figure 6(c) in the angular range from 55° to 115°. At high fields, the $J_c(\theta)$ curves are nearly symmetric around the ab-peak, while they become increasingly asymmetric with decreasing field. At 1 T, a clear shift of the maximum towards the surface (90°) is visible. For a more accurate quantitative description, we used the vortex-path model by N Long *et al* [44] based on the principle of entropy maximization. We fitted the data as a sum of two Lorentz-distribution peaks plus

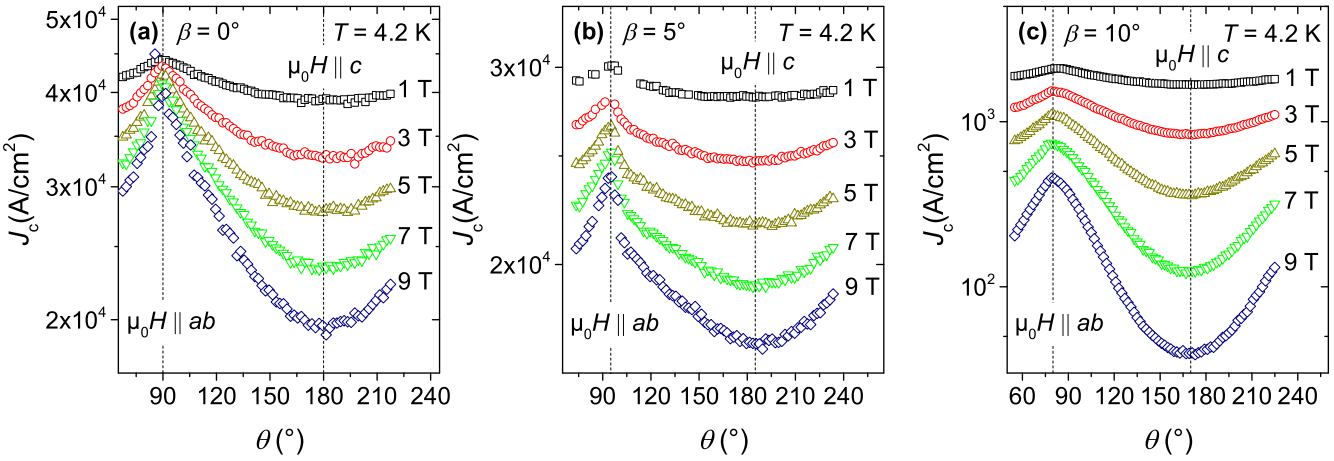

Figure 6. Angular dependent critical current densities in longitudinal direction in maximum Lorentz configuration for $Fe_{1+\delta}Se_{0.5}Te_{0.5}$ films of series 2 with vicinal angle β of (a) 0° (b) 5°, and (c) 10°. The *ab* peak is shifted by the angle β for both vicinal films; the shift direction is determined by the in plane sample mounting orientation.

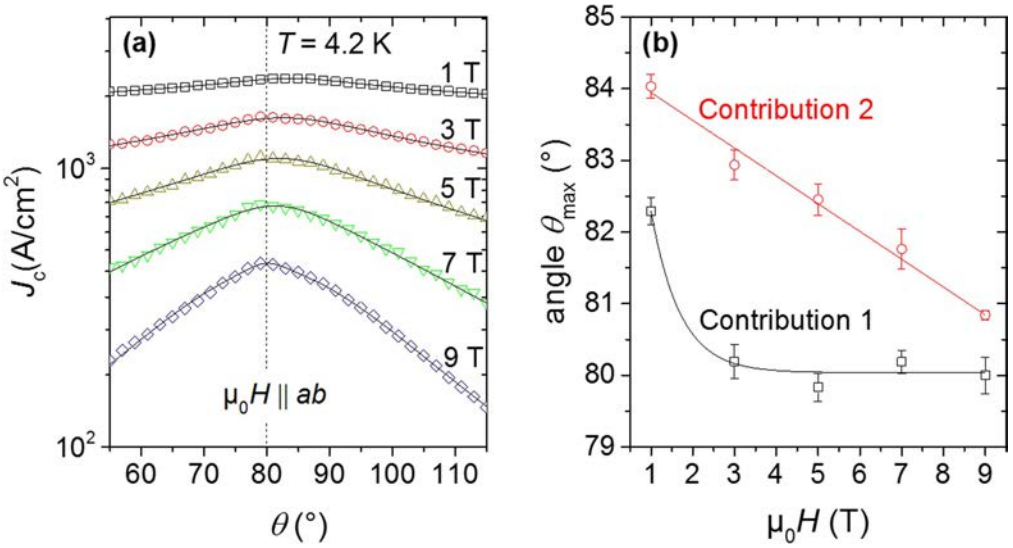

Figure 7. (a) $J_c(\theta)$ in the vicinity of the *ab* peak for the 10° vicinal $Fe_{1+\delta}Se_{0.5}Te_{0.5}$ thin film of series 2. The peaks are fitted with the vortex path model by equation (1). (b) Estimated maxima positions of contribution 1 and contribution 2. The solid lines are a guide to the eye.

constant background (equation (1))

$$J_c(\theta) = J_{c0} + \frac{J_{c1}\gamma_1}{\cos(\theta - \theta_1)^2 + \gamma_1^2 \sin(\theta - \theta_1)^2} + \frac{J_{c2}\gamma_2}{\cos(\theta - \theta_2)^2 + \gamma_2^2 \sin(\theta - \theta_2)^2}, \quad (1)$$

where J_{ci} are the J_c components, γ_i the peak widths, and θ_i the offset angles ($i = 0, 1, 2$). This function describes our data very well for all fields (figure 7(a)). In figure 7(b) the estimated maxima positions of the two contributions, i.e. 90°-θ_1 and 90°-θ_2, are plotted in dependence of the applied magnetic field. For contribution 1 we found a clear shift below 2 T. With an upper critical field in the range of 50 100 T [23] (and estimated using the data of the $FeSe_{0.5}Te_{0.5}/CaF_2$ film in [27]), this corresponds to a reduced field of $h \approx 0.02$, which agrees with the results of Silhanek *et al* [45] and Maiorov *et al* [43]. The direction of the shift (i.e. towards the sample surface) can be assigned to the 'geometry-dominated case' [45] and is explained by a misalignment between the internal and external magnetic field due to the energy minimization of the flux lines. This is in agreement with the theoretical prediction for low-anisotropy superconductor thin films with the given aspect ratio of *thickness*/*width* ~10 ^{4}, but is contrary to the experimental results of Trommler *et al* [18] for $BaFe_2As_2$ on Fe/MgO-buffered metal tapes and Maiorov *et al* [43] for YBCO on IBAD-MgO tapes. However, the situation is complicated by planar defects resulting in an additional influence and may lead to the linear peak shift of contribution 2. This effect should be subject of further studies, also on stoichiometric Fe(Se,Te) thin films.

Conclusion

We deposited reproducibly epitaxial superconducting $Fe_{1+\delta}Se_{0.5}Te_{0.5}$ thin films on 0°, 5°, 10°, 15° and 20° vicinal

cut CaF_2 single crystals by pulsed laser deposition. An alignment of the $Fe_{1+\delta}Se_{0.5}Te_{0.5}$ *c*-axis with the tilted substrate [001] axis was possible up to a vicinal angle of 10°. The use of vicinal cut substrates allowed the measurement of the resistivity anisotropy of thin films and therefore the measurement of the mass anisotropy parameter near T_c. The obtained values are in good agreement with reported data for single crystals. To investigate whether the tilted growth affects the flux pinning, we performed detailed J_c measurements for a 0° and a 5° vicinal film. We obtained that no effective correlated defects are generated by the vicinal growth, and pinning by normal point core defects dominates for $H||c$. For $H||ab$, pinning by extended planar defects is dominant for the 0° film, whereas point defects are more effective in the 5° vicinal film. For the 10° vicinal film, we furthermore observed a clear shift of the maxima position(s) in $J_c(\theta)$ with respect to the *ab*-planes. The sign of misalignment between the internal and external fields is as expected for low-anisotropy superconducting thin films.

Acknowledgments

The authors thank S Schwabe, S Richter, M Langer, F Yuan, F Kurth and V Grinenko for fruitful discussions, I Mönch for help with microbridge preparation, J Scheiter for the preparation and analysis of FIB cuts as well as M Kühnel and U Besold for technical support. We acknowledge the support of the European Union's Seventh Framework Program (FP7/2007 2013) under grant agreement 283204 (SUPER-IRON) and of the German Research Foundation (DFG) within the research training group GRK1621.

References

[1] Kamihara Y, Watanabe T, Hirano M and Hosono H 2008 *J. Am. Chem. Soc.* **130** 3296
[2] Rotter M, Tegel M and Johrendt D 2008 *Phys. Rev. Lett.* **101** 107006
[3] Hsu F C *et al* 2008 *Proc. Natl Acad. Sci. USA* **105** 14262
[4] Wang X C, Liu Q, Lv Y, Gao W, Yang L X, Yu R C, Li F Y and Jin C 2008 *Solid State Commun.* **148** 538
[5] Iida K, Hänisch J, Hühne R, Kurth F, Kidszun M, Haindl S, Werner J, Schultz L and Holzapfel B 2009 *Appl. Phys. Lett.* **95** 192501
[6] Si W, Lin Z W, Jie Q, Yin W G, Zhou J, Gu G, Johnson P D and Li Q 2009 *Appl. Phys. Lett.* **95** 052504
[7] Bellingeri E *et al* 2011 *J. Supercond. Nov. Magn.* **24** 35
[8] Engelmann J *et al* 2013 *Nat. Commun.* **4** 2877
[9] Iida K *et al* 2016 *Sci. Rep.* **6** 28390
[10] Haage T, Zegenhagen J, Li J Q, Habermeier H U, Cardona M, Jooss C, Warthmann R, Forkl A and Kronmüller H 1997 *Phys. Rev.* B **56** 8404
[11] Zahner T, Stierstorfer R, Rössler R, Pedarnig J D, Bäuerle D and Lengfellner H 1998 *Physica* C **298** 91
[12] Rössler R, Pedarnig J D and Jooss C 2001 *Physica* C **361** 13
[13] Xie Y Y, Wu J Z, Yun S H, Emergo R and Aga R 2004 *Appl. Phys. Lett.* **85** 70
[14] Polyanskii A A, Kametani F, Abraimov D, Gurevich A, Yamamoto A, Pallecchi I, Putti M, Zhuang C, Tan T and Xi X X 2014 *Phys. Rev.* B **90** 214509
[15] Lowndes D H, Christen D K, Klabunde C E, Wang Z L, Kroeger D M, Budai J D, Zhu S and Norton D P 1995 *Phys. Rev. Lett.* **74** 2355
[16] Sieger M *et al* 2017 *IEEE Trans. Appl. Supercond.* **27** 7500504
[17] Si W, Zhou J, Jie Q, Dimitrov I, Solovyov V, Johnson P D, Jaroszynski J, Matias V, Sheehan C and Li Q 2011 *Appl. Phys. Lett.* **98** 262509
[18] Trommler S, Hänisch J, Matias V, Hühne R, Reich E, Iida K, Haindl S, Schultz L and Holzapfel B 2012 *Supercond. Sci. Technol.* **25** 084019
[19] Iida K *et al* 2014 *Appl. Phys. Lett.* **105** 172602
[20] Mechin I, Berghuis P and Evetts J E 1998 *Physica* C **302** 102
[21] Emergo R L S, Wu J Z, Haugan T J and Barnes P N 2005 *Appl. Phys. Lett.* **87** 232503
[22] Sales B C, Sefat A S, McGuire M A, Jin R Y, Mandrus D and Mozharivskyj Y 2009 *Phys. Rev.* B **79** 094521
[23] Velasco Soto D, Rivera Gomez F J, Santillan Rodriguez C R, Saenz Hernandez R J, Botello Zubiate M E and Matutes Aquino J A 2013 *J. Appl. Phys.* **113** 17E138
[24] Palenzona *et al* 2012 *Supercond. Sci. Technol.* **25** 115018
[25] Huang S X, Chien C L, Thampy V and Broholm C 2010 *Phys. Rev. Lett.* **104** 217002
[26] Mele P, Matsumoto K, Fujita K, Yoshida Y, Kiss T, Ichinose A and Mukaida M 2012 *Supercond. Sci. Technol.* **25** 084021
[27] Yuan F F *et al* 2015 *Supercond. Sci. Technol.* **28** 065005
[28] Liu T J *et al* 2009 *Phys. Rev.* B **80** 174509
[29] Komiya S, Hanawa M, Tsukada I and Maeda A 2013 *J. Phys. Soc. Jpn.* **82** 064710
[30] Su T S, Yina Y W, Teng M L, Gong Z Z, Zhang M J and Li X G 2013 *J. Appl. Phys.* **114** 183901
[31] Sun Y, Tsuchiya Y, Taen T, Yamada T, Pyon S, Sugimoto A, Ekino T, Shi Z and Tamegai T 2014 *Sci. Rep.* **4** 4585
[32] Nelson J and Riley D 1945 *Proc. Phys. Soc.* **57** 160
[33] Noji T, Suzuki T, Abe H, Adachi T, Kato M and Koike Y 2010 *J. Phys. Soc. Jpn.* **79** 084711
[34] Klein T *et al* 2010 *Phys. Rev.* B **82** 184506
[35] Tsurkan V, Deisenhofer J, Günther A, Kant C, Klemm M, Krug von Nidda H A, Schrettle F and Loidl A 2011 *Eur. Phys. J.* B **79** 289
[36] Braccini *et al* 2013 *Appl. Phys. Lett.* **103** 172601
[37] Yuan P, Xu Z, Zhang H, Wang D, Ma Y, Zhang M and Li J 2015 *Supercond. Sci. Technol.* **28** 065009
[38] Sawada Y, Nabeshima F, Imai Y and Atsutaka Maeda A 2016 *J. Phys. Soc. Jpn.* **85** 073703
[39] Dew Hughes D 1974 *Phil. Mag.* **30** 293
[40] Si W, Han S J, Shi X, Ehrlich S N, Jaroszynski J, Goyal A and Li Q 2013 *Nat. Commun.* **4** 1347
[41] Bellingeri E *et al* 2014 *Supercond. Sci. Technol.* **27** 044007
[42] Yuan P S, Xu Z T, Ma Y W, Sun Y and Tamegai T 2016 *Supercond. Sci. Technol.* **29** 035013
[43] Maiorov B, Gibbons B J, Kreiskott S, Matias V and Jia Q X 2005 *IEEE Trans. Appl. Supercond.* **15** 2582
[44] Long N J *et al* 2008 *Supercond. Sci. Technol.* **21** 025007
[45] Silhanek A V, Civale L and Avila M A 2002 *Phys. Rev.* B **65** 174525